



JoVA: Unified Multimodal Learning for Joint Video-Audio Generation

Xiaohu Huang^{1,*} Hao Zhou^{2,*} Qiangpeng Yang²
Shilei Wen² Kai Han^{1,†}

¹The University of Hong Kong ²ByteDance

*Equal contribution †Corresponding author

Abstract

In this paper, we present **JoVA**, a unified framework for joint video-audio generation. Despite recent encouraging advances, existing methods face two critical limitations. First, most existing approaches can only generate ambient sounds and lack the capability to produce human speech synchronized with lip movements. Second, recent attempts at unified human video-audio generation typically rely on explicit fusion or modality-specific alignment modules, which introduce additional architecture design and weaken the model simplicity of the original transformers. To address these issues, JoVA employs joint self-attention across video and audio tokens within each transformer layer, enabling direct and efficient cross-modal interaction without the need for additional alignment modules. Furthermore, to enable high-quality lip-speech synchronization, we introduce a simple yet effective mouth-area loss based on facial keypoint detection, which enhances supervision on the critical mouth region during training without compromising architectural simplicity. Extensive experiments on benchmarks demonstrate that JoVA outperforms or is competitive with both unified and audio-driven state-of-the-art methods in lip-sync accuracy, speech quality, and overall video-audio generation fidelity. Our results establish JoVA as an elegant framework for high-quality multimodal generation. Project page: <https://visual-ai.github.io/jova>

Correspondence to: Kai Han at kaihanx@hku.hk, Xiaohu Huang at huangxiaohu@connect.hku.hk

1 Introduction

Recent years have witnessed significant progress in AI-driven content creation. Building upon the simplicity and scalability of image generation architectures [10, 31], related methods have been successfully extended to video and audio generation. For instance, [1, 21, 39, 53] achieves high-fidelity video synthesis, while [43] adapts diffusion models for diverse and high-quality audio generation, including ambient sounds, speech, and music. Advances in video-to-audio generation [3, 35, 41] and audio-driven avatar synthesis [2, 11, 12] have further promoted cross-modal representation learning.

Despite these developments, unified video-audio generation faces two critical challenges. First, most existing methods [25, 34, 42, 47, 55] can only generate ambient sounds and lack the capability to produce human speech synchronized with lip movements, severely limiting their applicability to human-centric scenarios. Second, inspired by the Google-Veo3 [7], recent attempts [27, 40] to address speech generation typically integrate pretrained video [39] and audio [14] models using additional fusion or cross-attention layers. While

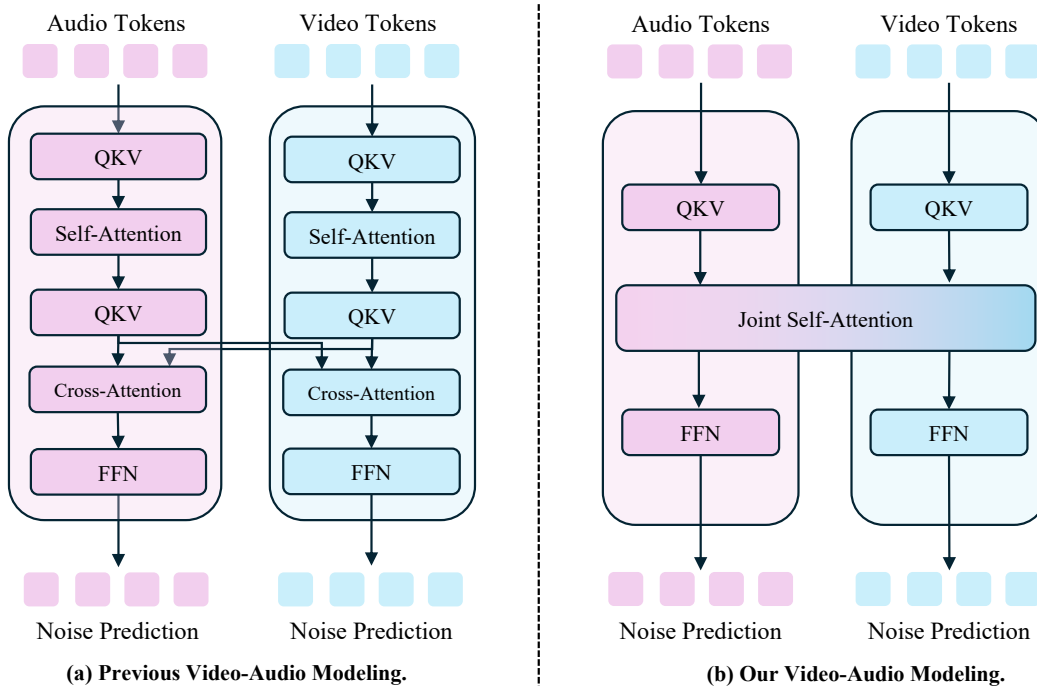


Figure 1 Architectural comparison of video-audio modeling approaches. (a) Previous methods rely on separate self-attention and cross-attention layers for video-audio fusion, resulting in complex and less extensible architectures. (b) JoVA uses a joint self-attention layer, allowing video and audio tokens to interact directly within a single layer, greatly simplifying the architecture.

these approaches achieve improved video-audio synchronization, the introduction of such modality-specific modules compromises the architectural simplicity of transformer-based models. As illustrated in Fig. 1(a), the redundant self-attention and cross-attention stacks not only increase architectural complexity but also hinder extensibility to new modalities or tasks due to the separate processing of multimodal tokens.

In contrast, we propose JoVA, a streamlined framework for unified video-audio generation that adheres to the core philosophy of transformer architectures—simplicity and extensibility. As illustrated in Fig. 1(b), we employ a unified architecture where video and audio tokens interact directly via joint self-attention within each layer, without introducing extra alignment or fusion modules. This design allows seamless cross-modal information exchange while maintaining architectural simplicity.

However, we observe that relying solely on joint attention presents difficulties in achieving precise lip-speech synchronization, a crucial requirement for natural human video-audio content creation. This challenge arises because the mouth region typically occupies only a small fraction of each video frame ($\sim 2.3\%$ in the training data), and the relevant audio features are temporally brief ($\sim 2.5\%$ in a 10-second video), resulting in sparse cross-modal associations. These factors make it difficult for a generic full-attention mechanism to capture the subtle correlations needed for precise alignment. To address this limitation, we introduce an area-specific loss strategy that leverages facial keypoint detection to localize the subject’s mouth region. By increasing the loss weight for this area during training, our method effectively guides the model to focus on learning the alignment between lip movements and speech. Notably, this solution is simple to implement and does not compromise the simplicity of the underlying architecture.

Experimental results on Universe-Bench [40] and UniAvatar-Bench datasets show that JoVA achieves superior/-competitive alignment and generation quality compared to previous unified [27, 40] and audio-driven [12, 44] approaches. We encourage readers to refer to the webpage for qualitative results.

We believe this plain architectural design offers a valuable foundation for unified multimodal generation and can be readily extended to incorporate more modalities and tackle more complex generative tasks. In

summary, our contributions are as follows:

- We present a unified architecture for video-audio generation with human speech capability, enabling full cross-modal interaction via joint attention without additional alignment modules.
- We introduce an area-specific loss on the mouth region to enhance lip-speech synchronization in a simple yet effective manner.
- Extensive experiments demonstrate that our approach achieves state-of-the-art alignment and generation quality, surpassing existing unified and audio-driven models.

2 Related Work

2.1 Video Generation Models

Recent advances in video generation have been driven by diffusion models, which initially relied on UNet-based architectures [33] and leveraged pre-trained image models [10] to address the scarcity of high-quality video data. The transition to transformer-based diffusion architectures [31], exemplified by Sora [26, 30], enabled large-scale training and significantly improved video fidelity. This shift spurred the development of new models such as Wan [6, 39], Waver [53], CogVideoX [50], and HunyuanVideo [21], along with several high-performing proprietary systems. Most state-of-the-art methods now employ a 3D variational autoencoder for spatio-temporal compression and a diffusion transformer operating in the latent space. Notably, Wan2.2 [39] and Waver [53] stand out for their ability to generate high-resolution, temporally coherent videos directly from text prompts or reference images. Overall, model performance in this field is closely tied to the scale and quality of training data, and these architectural advances have laid a strong foundation for unified multi-modal generation. In this work, we build upon Waver as our base model, aiming to achieve joint video-audio generation through a unified architecture.

2.2 Video-to-Audio and Audio-Driven Generation

Recent progress in cross-modal generation has led to significant advances in both video-to-audio (V2A) and audio-to-video (A2V) tasks. Previous approaches [2, 11, 12, 23] often follow a cascaded design: for audio-driven video synthesis, a text-to-speech (TTS) model first generates audio, which then conditions a separate video synthesis model to achieve lip synchronization. While effective for speech alignment, this two-stage pipeline suffers from modal decoupling, resulting in limited semantic coherence between audio and video. Conversely, video-to-audio methods [3, 15, 28, 35, 41, 54] generate soundtracks for silent videos, typically by conditioning on video features and text captions. They focus on ambient sounds or background music, employing cross-modal attention or contrastive training to improve temporal alignment. However, most existing pipelines still treat video and audio as separate streams, often requiring auxiliary modules for feature fusion or synchronization, which increases system complexity and limits generalization. In summary, despite notable progress in both directions, current approaches still face challenges in achieving seamless and unified video-audio generation. This motivates our work towards a more integrated and flexible multi-modal framework.

2.3 Joint Video-Audio Generation

Most of previous [17, 25, 34, 42, 47] unified video-audio generation methods focused on synthesizing ambient sounds using dual-branch architectures, where audio and video streams are processed separately and fused through explicit modules such as cross-attention or feature concatenation. While effective for basic cross-modal generation, these approaches introduce architectural fragmentation due to their reliance on modality-specific processing and complex fusion strategies. The advent of large-scale models like Google’s Veo3 [7] marked significant progress, demonstrating high-fidelity, temporally aligned joint generation of video and audio from text prompts. Building on this paradigm, recent open-source models such as UniVerse-1 [40] and Ovi [27] continue to follow the dual-branch approach, combining pretrained video and audio backbones with additional fusion or cross-attention layers. However, these methods still suffer from architectural inefficiencies and struggle to achieve fine-grained lip-speech synchronization, especially for human-centric content. To address

these challenges, we propose a streamlined, unified framework that enables direct cross-modal interaction within each transformer layer, eliminating the need for separate fusion modules.

3 Method

3.1 Preliminary

Our framework builds upon the Waver [53] video generation model, which employs a transformer-based diffusion architecture. For video encoding, we adopt the Wan2.1 VAE [39] to compress visual features in both spatial and temporal dimensions. Text prompts are processed through a combination of T5-XXL [4] and Qwen2.5-32B [48] encoders to provide rich semantic conditioning.

Following the MM-DiT architecture [9], Waver processes multi-modal inputs through a two-stage design: an initial multi-stream stage where modalities maintain separate parameters, followed by a single-stream stage where all modalities share the same parameters. Each stage consists of transformer blocks containing self-attention and feed-forward network (FFN) modules. For a given layer, the computation can be expressed as:

$$\mathbf{h}' = \text{SelfAttn}(\mathbf{h}) + \mathbf{h}, \quad \mathbf{h}'' = \text{FFN}(\mathbf{h}') + \mathbf{h}', \quad (1)$$

where $\mathbf{h} \in \mathbb{R}^{N \times D}$ denotes the input features with N tokens and dimension D .

For training, we employ the flow matching [24] framework, which provides a simple and effective approach for generative modeling. The training objective minimizes the difference between the predicted velocity field and the true flow velocity:

$$\mathcal{L}_{\text{FM}} = \mathbb{E}_{t, \mathbf{x}_0, \mathbf{x}_1, \mathbf{C}} \|v_\theta(t, \mathbf{C}, \mathbf{x}_t) - u(\mathbf{x}_t | \mathbf{x}_0, \mathbf{x}_1)\|^2, \quad (2)$$

where $t \sim \mathcal{U}[0, 1]$, $\mathbf{x}_0 \sim \mathcal{N}(0, \mathbf{I})$ is sampled noise, $\mathbf{x}_1 \sim q(\mathbf{x}_1, \mathbf{C})$ represents training data conditioned on \mathbf{C} (text and other modalities), $\mathbf{x}_t = t\mathbf{x}_1 + (1-t)\mathbf{x}_0$ defines the interpolation path, and $u(\mathbf{x}_t | \mathbf{x}_0, \mathbf{x}_1) = \mathbf{x}_1 - \mathbf{x}_0$ denotes the corresponding flow velocity.

3.2 JoVA Framework

3.2.1 Integrating Video and Audio Modality

To enable audio generation, we initialize an audio diffusion model by duplicating the pretrained video backbone parameters. We employ the MMAudio VAE [3] to extract audio spectrogram features, converting raw audio into a compact latent representation. This audio branch is then trained using the same flow matching objective in Eq. (2), but applied to audio data:

$$\mathcal{L}_{\text{audio}} = \mathbb{E}_{t, \mathbf{a}_0, \mathbf{a}_1, \mathbf{C}} \|v_\theta(t, \mathbf{C}, \mathbf{a}_t) - u(\mathbf{a}_t | \mathbf{a}_0, \mathbf{a}_1)\|^2, \quad (3)$$

where \mathbf{a}_t represents the audio latent at time t . Our training corpus includes both natural ambient sounds and human speech data (details in Sec. 3.3).

After pretraining both modalities separately, we unify them into a joint architecture for simultaneous video-audio generation. As illustrated in Fig. 2, we process the two pretrained models in parallel, with text prompt features fed into both branches. For video generation, we also support conditioning on a reference image \mathbf{I}_{ref} , which is encoded through the video VAE and concatenated with the noisy video latent along the channel dimension, following common practice in image-to-video generation [39, 53].

Within each transformer block, tokens from video, audio, and their respective text conditions are concatenated and processed through a shared self-attention mechanism:

$$[\mathbf{h}'_v; \mathbf{h}'_a; \mathbf{h}'_t] = \text{JointAttn}([\mathbf{h}_v; \mathbf{h}_a; \mathbf{h}_t]), \quad (4)$$

where \mathbf{h}_t contains text features for both video and audio branches. This design preserves the pretrained knowledge of each modality while enabling natural cross-modal information exchange among all modalities, achieving both representation preservation and feature fusion without introducing additional fusion modules.

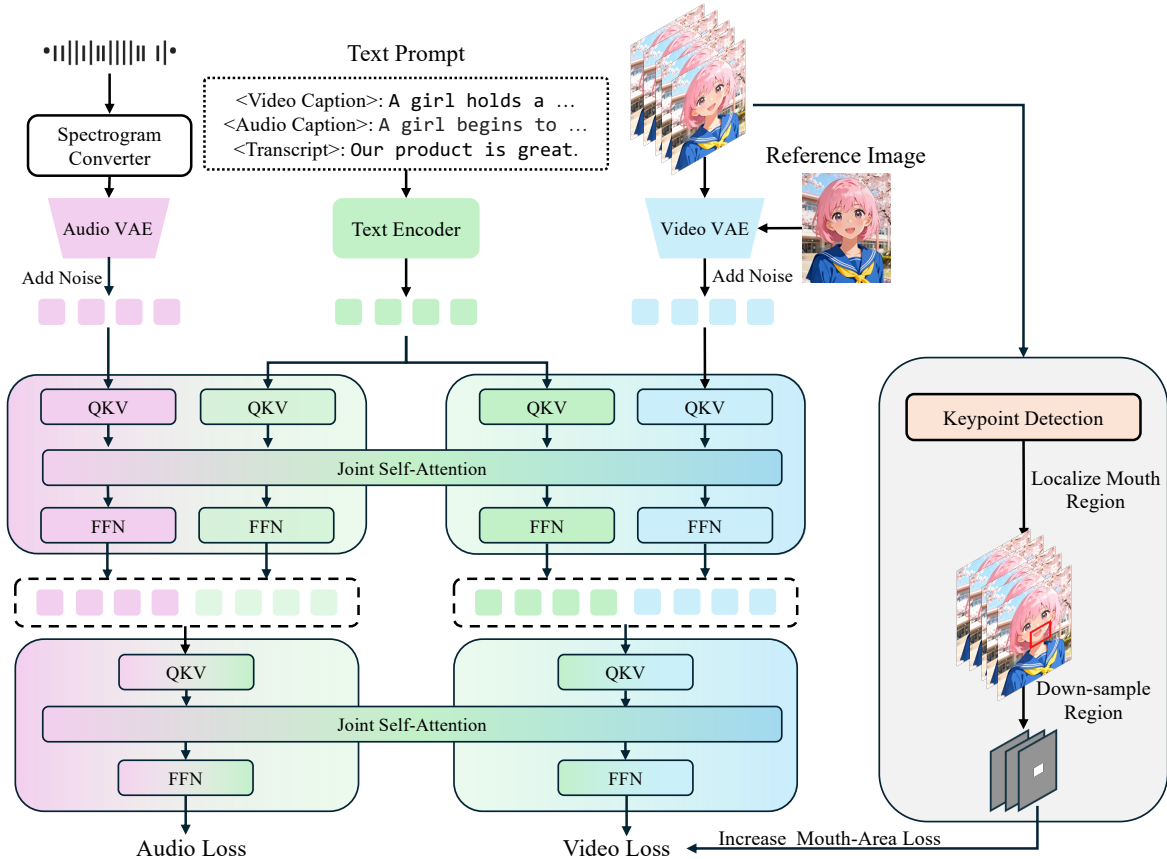


Figure 2 Overview of our JoVA framework. JoVA processes audio and video modalities through separate VAEs. Unlike previous methods that require explicit fusion modules, our architecture enables direct cross-modal interaction through joint self-attention layers, where audio (green), text (pink), and video (blue) tokens are processed equally together. We further enhance lip-speech synchronization through a mouth-area specific loss (right), which uses keypoint detection to localize the mouth region and applies increased supervision to this critical area without introducing additional architectural complexity. The character images shown are AIGC-generated.

The key advantage of this unified approach is its architectural simplicity. Unlike prior methods that rely on separate cross-attention layers or complex fusion networks, our joint self-attention mechanism allows video, audio, and text tokens to interact directly within the standard transformer framework. This not only reduces architectural complexity but also facilitates better gradient flow and more efficient training. Furthermore, to ensure temporal alignment between video and audio, we adopt the temporal-aligned RoPE (Rotary Position Embedding) from MMAudio [3], which synchronizes the positional encodings of both modalities along the temporal dimension.

While this unified architecture effectively handles general video-audio alignment, achieving fine-grained lip-speech synchronization for human-centric content requires additional supervision, which we address in the next section.

3.2.2 Mouth-Aware Supervision

To further enhance lip-speech synchronization, we introduce a targeted supervision strategy that emphasizes the mouth region during training. We first apply facial keypoint detection to the original video frames to localize the mouth region. Given the detected keypoints, we compute a bounding box that encompasses the mouth area in pixel space. This bounding box must then be mapped to the VAE latent space, which involves both spatial and temporal downsampling.

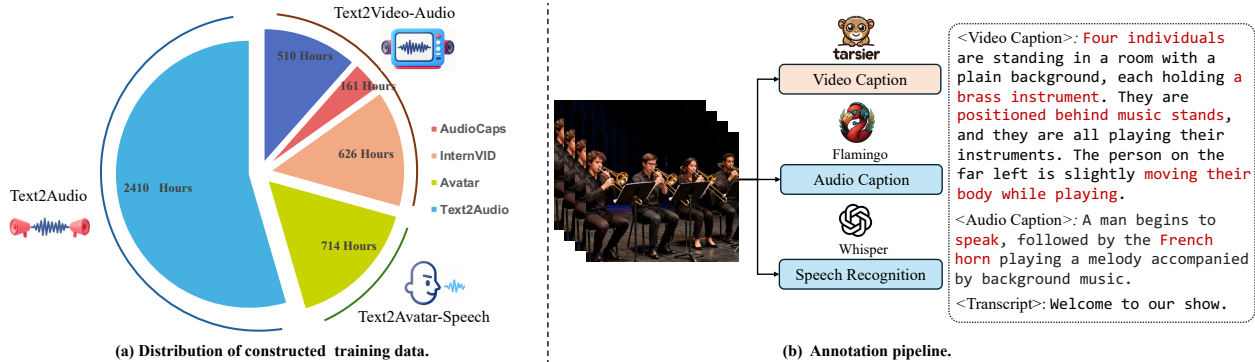


Figure 3 Overview of our training data construction and annotation pipeline. (a) Distribution of constructed training data across text2audio (ambient sounds), text2video-audio (paired video and audio from natural scenes), and text2avatar-speech (high-quality avatar video-speech pairs). (b) Annotation workflow for each video, including video captioning, audio captioning, and speech recognition, providing comprehensive text labels for multi-modal generation. The images shown are AIGC-generated.

For spatial mapping, we scale the bounding box proportionally according to the VAE’s spatial downsampling factor s . Specifically, for a bounding box (x_1, y_1, x_2, y_2) in pixel coordinates, the corresponding latent-space box becomes $(\lfloor x_1/s \rfloor, \lfloor y_1/s \rfloor, \lceil x_2/s \rceil, \lceil y_2/s \rceil)$.

The temporal downsampling is more nuanced, as it reduces the number of frames and thus the number of detected boxes. We employ a sliding window approach: using the temporal downsampling factor t_s as the window size, we slide across the sequence of detected boxes. Within each window, we compute the minimum bounding box that encompasses all mouth regions in that temporal segment:

$$\text{Box}_{\text{merged}} = \left(\min_i x_1^{(i)}, \min_i y_1^{(i)}, \max_i x_2^{(i)}, \max_i y_2^{(i)} \right), \quad (5)$$

where i indexes frames within the current window. This merged box serves as the mouth region for the corresponding VAE latent frame. Through empirical validation on sample data (see App. A), we confirm that this approach accurately localizes the mouth region in latent space.

With the mouth region identified, we apply increased supervision specifically to these areas. Our final training objective combines three components:

$$\mathcal{L}_{\text{total}} = \mathcal{L}_{\text{video}} + \mathcal{L}_{\text{audio}} + \lambda \mathcal{L}_{\text{mouth}}, \quad (6)$$

where $\mathcal{L}_{\text{video}}$ and $\mathcal{L}_{\text{audio}}$ are computed using Eq. (2) and Eq. (3) respectively, $\mathcal{L}_{\text{mouth}}$ applies the same flow matching loss but only to the mouth region of the video latent:

$$\mathcal{L}_{\text{mouth}} = \mathbb{E}_{t, \mathbf{v}_0, \mathbf{v}_1, \mathbf{C}} \|v_\theta(t, \mathbf{C}, \mathbf{v}_t)_{\mathcal{M}} - u(\mathbf{v}_t | \mathbf{v}_0, \mathbf{v}_1)_{\mathcal{M}}\|^2, \quad (7)$$

where \mathbf{v}_t denotes the video latent at time t , \mathcal{M} denotes the mouth region mask, and λ is a weighting coefficient that controls the emphasis on mouth-area supervision. This simple yet effective strategy guides the model to learn fine-grained lip-speech alignment without compromising the architectural simplicity of our unified framework.

3.3 Construction of Training Data

To support unified video-audio generation across diverse scenarios, as seen in see Fig. 3, we construct a training dataset comprising three components: text-to-audio (text2audio), text-to-video-audio (text2video-audio), and text-to-avatar-speech (text2avatar-speech) data. The text2audio subset includes approximately 2,410 hours of audio collected from Clotho [8], AudioCaps [19], and WaveCaps [29], covering a wide variety of natural ambient sounds and events. The text2video-audio subset consists of 1,297 hours of paired video and audio from InternVID [45], and AudioCaps [19], enabling the model to learn cross-modal correspondences

between visual content and sound in natural scenes. To facilitate precise modeling of human speech and lip synchronization, we construct a high-fidelity audio-visual dataset consisting of approximately 700 hours of talking head videos. These videos were collected from publicly available sources and underwent a rigorous data cleaning pipeline to filter out low-quality samples and ensure audio-visual synchronization.

For each video sample, we design a multi-stage annotation pipeline to provide high-quality supervision for multi-modal learning. First, we employ the Tarsier2 [51] model to generate detailed video captions, describing not only the salient objects and their spatial arrangements, but also relevant actions and interactions within the visual scene. Second, we apply the Audio-flamingo3 [13] model to produce audio captions, which summarize the main auditory events and sources present in the corresponding audio track, including both speech and non-speech components. Third, to enable precise modeling of human speech and facilitate lip-speech synchronization, we utilize Whisper [32] for automatic speech recognition (ASR), extracting accurate transcripts of any spoken content within the audio.

This tri-level annotation enriches each sample with structured semantic information from complementary perspectives: the video caption provides a global visual context, the audio caption offers a summary of the soundscape, and the transcript supplies fine-grained linguistic details. Such comprehensive labeling not only supports general video-audio generation but also provides the necessary supervision for challenging tasks such as avatar speech alignment and naturalistic talking face generation.

4 Experiments

4.1 Datasets and Evaluation Metrics

Datasets. We evaluate our method on two benchmarks. First, we introduce **UniAvatar-Bench**, a curated evaluation set consisting of 100 diverse samples. These samples are strictly selected from publicly available datasets and are carefully selected to ensure no overlap with our training data. Second, we employ **Verse-Bench** [40], which contains 600 image-text prompt pairs spanning a wide range of audio categories including human speech, animal vocalizations, instrumental music, and natural ambient sounds.

Evaluation Metrics. Following the evaluation protocol of Universe [40], we assess our model from four perspectives: joint video-audio quality, text-to-speech accuracy, audio generation quality, and video generation fidelity. For video-audio alignment, we measure lip-sync accuracy using SyncNet [5] to calculate confidence scores (LSE-C). Text-to-speech quality is evaluated through Word Error Rate (WER) by transcribing generated audio with Whisper-large-v3 [32]. Video quality is assessed through Motion Score (MS) calculated from RAFT-detected [37] optical flow, Aesthetic Score (AS) averaging MANIQA [49] fidelity and aesthetic quality from aesthetic-predictor-v2-5 and Musiq [18], and ID consistency measuring DINOv3 [36] feature similarity between reference images and generated frames. For audio generation, we evaluate distributional similarity using Fréchet Distance (FD) and Kullback-Leibler (KL) divergence on PANNs [20] and PaSST [22] features, semantic consistency via LAION-CLAP [46] scores, and quality metrics including Inception Score (IS) and AudioBox-Aesthetics [38] measures for Production Quality (PQ), Production Complexity (PC), Content Enjoyment (CE), and Content Usefulness (CU).

4.2 Implementation Details

Unless stated, our framework builds upon the Waver [53] 12B model as the base architecture. We adopt a two-stage training strategy: in the first stage, we train individual modality branches on collected audio-video data using a batch size of 256 and a fixed learning rate of 1×10^{-4} for 80K steps. In the second stage, we perform joint video-audio training with a batch size of 32 and learning rate of 5×10^{-5} for 50K steps to enable cross-modal interaction. During inference, we apply classifier-free guidance [16] with a weight of 10.0 for both video and audio generation to enhance generation quality.

4.3 Comparison with State-of-the-Art Models

We compare our method against two categories of approaches: (1) audio-driven generation methods, where we use ground-truth audio to drive video synthesis for fair comparison of conditional generation capability,

Table 1 Performance comparison on UniAvatar-Bench. The results of other methods are reproduced with their official code. The audio inputs for audio-driven models are from ground-truths.

Method	Audio-Video	TTS	Audio							Video		
	LSE-C \uparrow	WER \downarrow	FD \downarrow	KL \downarrow	CS \uparrow	CE \uparrow	CU \uparrow	PC \downarrow	PQ \uparrow	MS \uparrow	AS \uparrow	ID \uparrow
<i>Audio-driven Generation</i>												
Fantasy-Talking [44]	3.10	-	-	-	-	-	-	-	-	0.22	0.44	0.87
Wan-S2V [12]	6.43	-	-	-	-	-	-	-	-	0.82	0.44	0.72
<i>Joint Video-Audio Generation</i>												
Universe-1 [40]	1.62	0.37	1.04	0.83	0.16	3.68	3.90	2.12	4.39	0.43	0.42	0.82
OVI [27]	6.41	0.23	0.75	0.66	0.30	5.00	5.67	1.75	5.77	0.94	0.41	0.75
JoVA	6.64	0.18	0.69	0.63	0.28	5.46	6.20	1.71	6.45	0.98	0.47	0.78

including FantasyTalking [44] and Wan-S2V [12]; (2) joint video-audio generation methods, including the recent Universe-1 [40] and OVI [27].

Table 1 presents results on UniAvatar-Bench. Our method achieves the best overall performance, particularly excelling in the critical lip-sync metric (LSE-C) with a score of 6.64, surpassing both joint generation methods OVI (6.41) and Universe-1 (1.62), and even outperforming the audio-driven model Wan-S2V (6.43). This demonstrates the effectiveness of our mouth-area supervision strategy in achieving precise lip synchronization. For text-to-speech quality, our method achieves the lowest WER of 0.18, significantly outperforming Universe-1 (0.37) and OVI (0.23), indicating superior speech synthesis accuracy. In audio generation, we obtain the best scores across all metrics, with FD of 0.69, KL of 0.63, CE of 5.46, CU of 6.20, and particularly strong PQ of 6.45, substantially surpassing competing methods. For video quality, our method achieves the highest motion score (0.98) and aesthetic score (0.47), demonstrating superior dynamic modeling and visual fidelity. While our identity consistency (0.78) is slightly lower than audio-driven methods, it represents a reasonable trade-off given our model’s capability to generate both modalities jointly from text prompts, which is a significantly more challenging task.

Table 2 Performance comparison on Verse-Bench. The performance of OVI is reproduced using the official code.

Method	Audio-Video	TTS	Audio							Video		
	LSE-C \uparrow	WER \downarrow	FD \downarrow	KL \downarrow	CS \uparrow	CE \uparrow	CU \uparrow	PC \downarrow	PQ \uparrow	MS \uparrow	AS \uparrow	ID \uparrow
<i>Audio-driven Generation</i>												
FantasyTalking [44]	2.68	-	-	-	-	-	-	-	-	0.07	0.42	0.87
Wan-S2V [12]	6.49	-	-	-	-	-	-	-	-	0.17	0.46	0.89
<i>Joint Video-Audio Generation</i>												
Universe [40]	1.62	0.18	1.25	2.70	0.16	3.53	4.61	2.49	5.20	0.20	0.47	0.89
OVI [27]	6.61	0.12	0.97	2.23	0.20	3.95	5.60	2.09	6.20	0.55	0.47	0.86
JoVA	6.51	0.11	1.10	2.16	0.23	4.00	5.24	2.23	5.61	0.80	0.48	0.86

On Verse-Bench (Table 2), our method continues to demonstrate strong performance across diverse scenarios. We achieve the lowest WER (0.11), confirming robust speech accuracy. Our LSE-C score of 6.51 slightly underperforms OVI (6.41) while substantially outperforming Universe (1.62), validating the generalization of our lip-sync approach. In audio generation, we achieve competitive FD (1.10) and the best KL score (2.16) while attaining the highest CS of 0.23 and CE of 4.00 among all methods. For video generation, our method

achieves the highest motion score (0.80) and aesthetic score (0.48), demonstrating superior ability to generate dynamic and visually appealing content while preserving identity consistency (0.86) comparable to leading methods. Notably, we maintain balanced performance across all metrics without sacrificing quality in any dimension.

4.4 Diagnostic Study

Table 3 Effect of using mouth-aware loss λ .

λ	LSE-C \uparrow	WER \downarrow	FD \downarrow	KL \downarrow	PQ \uparrow	AS \uparrow
0.0	1.39	0.18	0.68	0.64	6.50	0.47
2.0	6.50	0.17	0.67	0.62	6.48	0.47
5.0	6.64	0.18	0.69	0.63	6.45	0.47
8.0	6.63	0.17	0.69	0.62	6.43	0.47

Table 4 Effect of using temporal-aligned RoPE (TA-RoPE).

TA-RoPE	LSE-C \uparrow	WER \downarrow	FD \downarrow	KL \downarrow	PQ \uparrow	AS \uparrow
\times	6.58	0.17	0.58	0.64	6.45	0.46
\checkmark	6.64	0.18	0.69	0.63	6.45	0.47

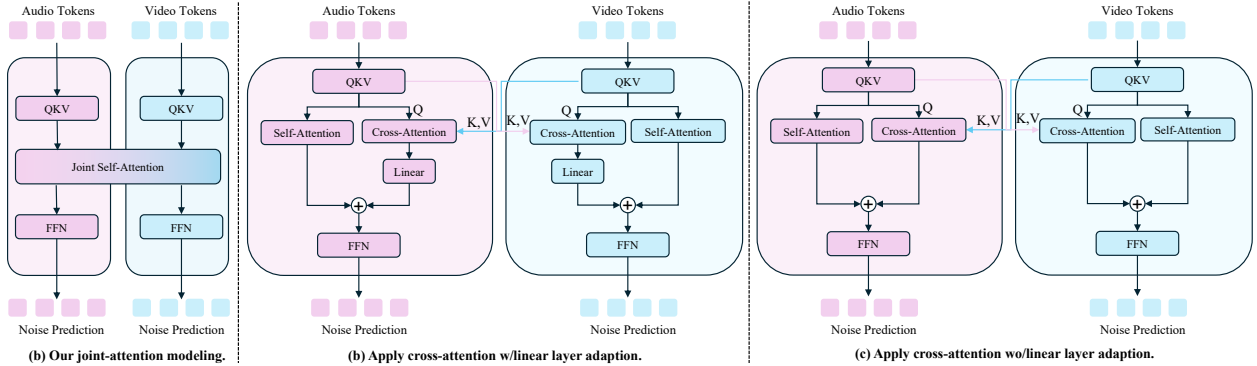


Figure 4 Comparison of different audio-video fusion strategies. (a) Our joint attention mechanism processes audio and video tokens together through unified self-attention, enabling bidirectional information exchange in a single layer. (b) Cross-attention with linear layer adaptation reuses the original attention parameters to compute cross-modal attention in parallel with self-attention, with a linear layer adapting the cross-attention output before merging with self-attention results. (c) Cross-attention without linear layer adaptation directly adds the cross-attention output to self-attention without adaptation.

Effectiveness of Mouth-Aware Loss. We first investigate the impact of the mouth-aware loss weight λ in Eq.(6). As shown in Table 3, increasing λ from 0.0 dramatically improves lip-sync accuracy (LSE-C from 1.39 to 6.50), demonstrating the critical role of targeted supervision on the mouth region. Without mouth-aware loss ($\lambda = 0.0$), the model fails to learn fine-grained lip-speech alignment through joint attention alone. The optimal performance is achieved at $\lambda = 5.0$ (LSE-C: 6.64), where the model effectively balances lip-sync precision with overall generation quality. Further increasing λ to 8.0 leads to marginal degradation (LSE-C: 6.63). Notably, audio quality metrics (WER, KL, PQ) and AS remain stable across different λ values, confirming that our mouth-aware supervision strategy enhances lip-sync without sacrificing general audio-visual quality. The substantial improvement from $\lambda = 0.0$ to $\lambda = 2.0$ (LSE-C: 1.39 \rightarrow 6.50) highlights the necessity of explicit mouth-region guidance for achieving precise synchronization.

Temporal-Aligned RoPE vs. Non-Aligned RoPE. We examine the importance of temporal-aligned RoPE for cross-modal synchronization. As shown in Table 4, using aligned RoPE—where video and audio tokens share synchronized positional encodings along the temporal dimension—presents a clear trade-off. With temporal alignment, the model achieves better lip-sync accuracy (LSE-C: 6.64 vs. 6.58), while maintaining comparable performance on most other metrics (WER, KL, PQ, AS). However, it incurs a slight degradation in FD from 0.69 to 0.58. Given that precise lip-speech synchronization is critical for human-centric video generation and the primary focus of our work, we adopt the temporal-aligned RoPE despite the minor FD trade-off. This design choice prioritizes temporal correspondence—enabling the model to establish accurate frame-level

Table 5 Performance comparison of using joint self-attention and cross-attention modules on UniAvatar-Bench.

Method	Audio-Video	TTS	Audio						Video			
	LSE-C \uparrow	WER \downarrow	FD \downarrow	KL \downarrow	CS \uparrow	CE \uparrow	CU \uparrow	PC \downarrow	PQ \uparrow	MS \uparrow	AS \uparrow	ID \uparrow
Cross-attention w/ linear	1.63	0.27	0.69	0.64	0.27	5.38	6.07	1.79	6.26	1.00	0.46	0.74
Cross-attention w/o linear	6.49	0.29	0.70	0.60	0.28	5.28	5.90	1.82	6.08	1.01	0.45	0.75
Joint self-attention	6.64	0.18	0.69	0.63	0.28	5.46	6.20	1.71	6.45	0.98	0.47	0.78

alignment between lip movements and speech—over marginal improvements in visual diversity. The results suggest that explicit temporal encoding provides a valuable inductive bias for cross-modal synchronization, which is beneficial for generating perceptually convincing talking head videos.

Comparison of Joint Self-Attention and Cross-Attention To validate the effectiveness of our joint self-attention design, we compare it with two cross-attention variants. As illustrated in Fig. 4, the key difference lies in how audio and video modalities interact. Our design processes both audio and video tokens together in a unified self-attention mechanism, allowing natural bidirectional information flow between modalities in a single layer. In contrast, cross-attention approaches compute cross-modal attention in parallel with self-attention by reusing the original attention parameters, where audio tokens attend to video tokens and vice versa. The variant with linear adaptation adds a linear projection layer to adapt the cross-attention output before combining it with the self-attention result, while the variant without linear adaptation directly adds the cross-attention output to self-attention.

Tab. 5 presents quantitative comparisons among the three fusion strategies. Our joint self-attention achieves the best LSE-C score (6.64) and significantly lower WER (0.18), demonstrating superior lip-speech synchronization compared to cross-attention variants. The cross-attention with linear adaptation performs particularly poorly (LSE-C: 1.63), suggesting that the linear adaptation layer may introduce semantic misalignment when combining self-attention and cross-attention outputs. For audio quality, joint self-attention achieves the best overall performance with highest scores in CE (5.46), CU (6.20), and PQ (6.45), along with lowest PC (1.71). In terms of video quality, while all methods achieve comparable motion score ($MS \approx 1.0$), joint self-attention excels in aesthetic quality (AS: 0.47) and identity preservation (ID: 0.78). These results validate our design choice, demonstrating that unified multimodal processing through joint self-attention is essential for achieving high-quality, synchronized audio-visual generation without introducing additional parameters.

Additional Experiments with the Waver-1.6B Model To further analyze the scalability and efficiency of our JoVA framework, we additionally conduct experiments using a smaller Waver-1.6B backbone. Since JoVA adopts separate video and audio branches (each with its own backbone), the total parameter counts for the 1.6B and 12B backbones are 3.2B ($1.6B \times 2$) and 24B ($12B \times 2$), respectively.

Tab. 6 summarizes the results on UniAvatar-Bench, together with comparisons to Universe-1 and OVI. Even

Table 6 Performance comparison with other video-audio generation models on UniAvatar-Bench. The results of other methods are reproduced with their official code. The number of training samples of Universe-1 and OVI is taken from [52]. **For JoVA, the parameter count is the sum of video and audio branches, i.e., two times the Waver backbone size ($1.6B \times 2 = 3.2B$ and $12B \times 2 = 24B$).**

Method	Training Samples	Params	Audio-Video	TTS	Audio						Video			
			LSE-C \uparrow	WER \downarrow	FD \downarrow	KL \downarrow	CS \uparrow	CE \uparrow	CU \uparrow	PC \downarrow	PQ \uparrow	MS \uparrow	AS \uparrow	ID \uparrow
Universe-1 [40]	6.4M	7.1B	1.62	0.37	1.04	0.83	0.16	3.68	3.90	2.12	4.39	0.43	0.42	0.82
OVI [27]	30.7M	10.9B	6.41	0.23	0.75	0.66	0.30	5.00	5.67	1.75	5.77	0.94	0.41	0.75
JoVA	1.9M	3.2B	6.20	0.19	0.68	0.58	0.28	5.36	6.04	1.75	6.27	1.05	0.46	0.75
JoVA	1.9M	24B	6.64	0.18	0.69	0.63	0.28	5.46	6.20	1.71	6.45	0.98	0.47	0.78

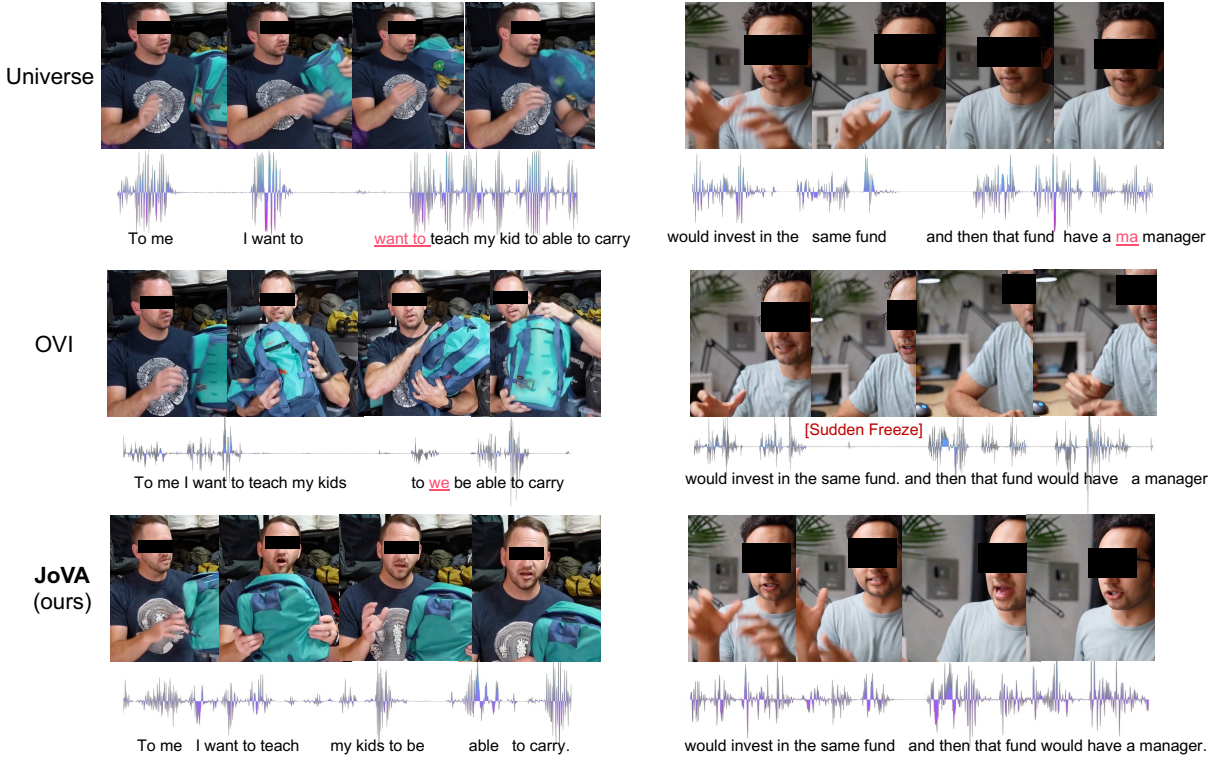


Figure 5 Qualitative comparison of speech generation and lip-sync quality. Generated video frames with audio waveforms and ASR transcriptions. Red underlines indicate speech recognition errors. Universe omits words, OVI shows freezing artifacts and mispronunciations, while our JoVA produces accurate speech with precise lip-sync alignment. The eyes have been obscured to protect the subject’s identity.

with only 3.2B parameters and 1.9M training samples, JoVA achieves a strong LSE-C score of 6.20, which significantly outperforms Universe-1 (1.62; 7.1B parameters; 6.4M samples) and is competitive with OVI (6.41; 10.9B; 30.7M). JoVA (3.2B) also achieves the lowest FD (0.68), and the best MS (1.05) among all methods, further demonstrating strong audio-visual alignment and video quality even with limited capacity.

As shown in the main results, JoVA (24B) achieves the best or comparable performance across all metrics: LSE-C increases to 6.64, PQ improves to 6.45, and WER drops to 0.18. JoVA (24B) also achieves the top results in KL (0.63), CE (5.46), CU (6.20), PC (1.71), AS (0.47), and ID (0.78), and remains highly competitive in all other metrics.

These results demonstrate that JoVA’s joint self-attention and mouth-aware loss provide significant improvements in cross-modal alignment and generation quality, even at a small model scale, while consistently benefiting from increased model capacity. Notably, Universe-1 lags behind in lip-sync and multi-modal generation, despite having more parameters and training data.

Furthermore, the high efficiency of JoVA’s architecture enables strong cross-modal generation even in low-resource or small-model scenarios, showing great potential for practical deployment.

4.5 Quantitative Results

Figure 5 presents qualitative comparisons of video-audio generation quality. We visualize generated frames alongside their audio waveforms and automatic speech recognition (ASR) results, with recognition errors underlined in red. Universe produces incomplete speech with missing words (e.g., omitting "want to"), indicating poor audio generation quality. OVI suffers from temporal consistency issues, exhibiting sudden freezing artifacts and mispronunciations (e.g., generating "we" instead of "to"). In contrast, our JoVA generates

smooth, natural speech with accurate word pronunciation and maintains precise lip-speech synchronization throughout the sequence. The aligned audio waveforms and correct ASR transcriptions demonstrate JoVA’s superior capability in joint video-audio generation with proper cross-modal alignment. Please see the video demos in the supplementary materials.

5 Conclusion

In this paper, we proposed JoVA, a unified framework for joint video-audio generation with human speech capability. Unlike existing methods that rely on complex fusion or alignment modules, JoVA employs joint self-attention for direct cross-modal interaction, maintaining architectural simplicity. To enhance lip-speech synchronization, we introduce a simple yet effective mouth-area specific loss strategy. Extensive experiments on UniAvatar-Bench and Universe-Bench demonstrate that JoVA achieves state-of-the-art performance in lip-sync accuracy, speech quality, and overall generation fidelity, outperforming both unified and audio-driven baselines.

We believe this plain architectural design provides a foundation for multimodal generation research. Its simplicity makes it well-suited for extension to additional modalities and more complex generative tasks, advancing towards universal multimodal content creation.

6 Declaration

All datasets, images and videos of designed character portraits used in this paper are solely for research purposes. In addition, the datasets and models employed in this paper are also exclusively for research use and will not be integrated into any products of ByteDance.

Acknowledgments

This work is supported by Hong Kong Research Grant Council - General Research Fund (Grant No. 17211024).

References

- [1] Andreas Blattmann, Tim Dockhorn, Sumith Kulal, Daniel Mendelevitch, Maciej Kilian, Dominik Lorenz, Yam Levi, Zion English, Vikram Voleti, Adam Letts, et al. Stable video diffusion: Scaling latent video diffusion models to large datasets. arXiv preprint arXiv:2311.15127, 2023.
- [2] Yi Chen, Sen Liang, Zixiang Zhou, Ziyao Huang, Yifeng Ma, Junshu Tang, Qin Lin, Yuan Zhou, and Qinglin Lu. Hunyuanvideo-avatar: High-fidelity audio-driven human animation for multiple characters. arXiv preprint arXiv:2505.20156, 2025.
- [3] Ho Kei Cheng, Masato Ishii, Akio Hayakawa, Takashi Shibuya, Alexander Schwing, and Yuki Mitsufuji. Mmaudio: Taming multimodal joint training for high-quality video-to-audio synthesis. In CVPR, 2025.
- [4] Hyung Won Chung, Noah Constant, Xavier Garcia, Adam Roberts, Yi Tay, Sharan Narang, and Orhan Firat. Unimax: Fairer and more effective language sampling for large-scale multilingual pretraining. arXiv preprint arXiv:2304.09151, 2023.
- [5] Joon Son Chung and Andrew Zisserman. Out of time: automated lip sync in the wild. In ACCV, 2016.
- [6] Alibaba Cloud. Wan2.5. <https://wan.video/>, 2025.
- [7] Google DeepMind. Veo3. <https://deepmind.google/models/veo/>, 2025.
- [8] Konstantinos Drossos, Samuel Lipping, and Tuomas Virtanen. Clotho: An audio captioning dataset. In ICASSP, 2020.
- [9] Patrick Esser, Sumith Kulal, Andreas Blattmann, Rahim Entezari, Jonas Müller, Harry Saini, Yam Levi, Dominik Lorenz, Axel Sauer, Frederic Boesel, et al. Scaling rectified flow transformers for high-resolution image synthesis. In ICML, 2024.
- [10] Patrick Esser, Sumith Kulal, Andreas Blattmann, Rahim Entezari, Jonas Müller, Harry Saini, Yam Levi, Dominik Lorenz, Axel Sauer, Frederic Boesel, et al. Scaling rectified flow transformers for high-resolution image synthesis. In ICML, 2024.
- [11] Qijun Gan, Ruizi Yang, Jianke Zhu, Shaofei Xue, and Steven Hoi. Omniaavatar: Efficient audio-driven avatar video generation with adaptive body animation. arXiv preprint arXiv:2506.18866, 2025.
- [12] Xin Gao, Li Hu, Siqi Hu, Mingyang Huang, Chaonan Ji, Dechao Meng, Jinwei Qi, Penchong Qiao, Zhen Shen, Yafei Song, et al. Wan-s2v: Audio-driven cinematic video generation. arXiv preprint arXiv:2508.18621, 2025.
- [13] Arushi Goel, Sreyan Ghosh, Jaehyeon Kim, Sonal Kumar, Zhifeng Kong, Sang-gil Lee, Chao-Han Huck Yang, Ramani Duraiswami, Dinesh Manocha, Rafael Valle, et al. Audio flamingo 3: Advancing audio intelligence with fully open large audio language models. arXiv preprint arXiv:2507.08128, 2025.
- [14] Junmin Gong, Sean Zhao, Sen Wang, Shengyuan Xu, and Joe Guo. Ace-step: A step towards music generation foundation model. arXiv preprint arXiv:2506.00045, 2025.
- [15] Moayed Haji-Ali, Willi Menapace, Aliaksandr Siarohin, Ivan Skorokhodov, Alper Canberk, Kwot Sin Lee, Vicente Ordonez, and Sergey Tulyakov. Av-link: Temporally-aligned diffusion features for cross-modal audio-video generation. arXiv preprint arXiv:2412.15191, 2024.
- [16] Jonathan Ho and Tim Salimans. Classifier-free diffusion guidance. arXiv preprint arXiv:2207.12598, 2022.
- [17] Masato Ishii, Akio Hayakawa, Takashi Shibuya, and Yuki Mitsufuji. A simple but strong baseline for sounding video generation: Effective adaptation of audio and video diffusion models for joint generation. arXiv preprint arXiv:2409.17550, 2024.
- [18] Junjie Ke, Qifei Wang, Yilin Wang, Peyman Milanfar, and Feng Yang. Musiq: Multi-scale image quality transformer. In ICCV, 2021.
- [19] Chris Dongjoo Kim, Byeongchang Kim, Hyunmin Lee, and Gunhee Kim. Audiocaps: Generating captions for audios in the wild. In ACL, 2019.
- [20] Qiuqiang Kong, Yin Cao, Turab Iqbal, Yuxuan Wang, Wenwu Wang, and Mark D Plumbley. Panns: Large-scale pretrained audio neural networks for audio pattern recognition. TASLPRO, 2020.

- [21] Weijie Kong, Qi Tian, Zijian Zhang, Rox Min, Zuozhuo Dai, Jin Zhou, Jiangfeng Xiong, Xin Li, Bo Wu, Jianwei Zhang, et al. Hunyuanvideo: A systematic framework for large video generative models. [arXiv preprint arXiv:2412.03603](#), 2024.
- [22] Khaled Koutini, Jan Schlüter, Hamid Eghbal-Zadeh, and Gerhard Widmer. Efficient training of audio transformers with patchout. [arXiv preprint arXiv:2110.05069](#), 2021.
- [23] Gaojie Lin, Jianwen Jiang, Jiaqi Yang, Zerong Zheng, and Chao Liang. Omnihuman-1: Rethinking the scaling-up of one-stage conditioned human animation models. [arXiv preprint arXiv:2502.01061](#), 2025.
- [24] Yaron Lipman, Ricky TQ Chen, Heli Ben-Hamu, Maximilian Nickel, and Matt Le. Flow matching for generative modeling. [arXiv preprint arXiv:2210.02747](#), 2022.
- [25] Kai Liu, Wei Li, Lai Chen, Shengqiong Wu, Yanhao Zheng, Jiayi Ji, Fan Zhou, Rongxin Jiang, Jiebo Luo, Hao Fei, et al. Javisdit: Joint audio-video diffusion transformer with hierarchical spatio-temporal prior synchronization. [arXiv preprint arXiv:2503.23377](#), 2025.
- [26] Yixin Liu, Kai Zhang, Yuan Li, Zhiling Yan, Chujie Gao, Ruoxi Chen, Zhengqing Yuan, Yue Huang, Hanchi Sun, Jianfeng Gao, et al. Sora: A review on background, technology, limitations, and opportunities of large vision models. [arXiv preprint arXiv:2402.17177](#), 2024.
- [27] Chetwin Low, Weimin Wang, and Calder Katyal. Ovi: Twin backbone cross-modal fusion for audio-video generation. [arXiv preprint arXiv:2510.01284](#), 2025.
- [28] Simian Luo, Chuanhao Yan, Chenxu Hu, and Hang Zhao. Diff-foley: Synchronized video-to-audio synthesis with latent diffusion models. [NeurIPS](#), 2023.
- [29] Xinhao Mei, Chutong Meng, Haohe Liu, Qiuqiang Kong, Tom Ko, Chengqi Zhao, Mark D Plumbley, Yuexian Zou, and Wenwu Wang. Wavcaps: A chatgpt-assisted weakly-labelled audio captioning dataset for audio-language multimodal research. [TASLPRO](#), 2024.
- [30] Openai. Sora2. <https://openai.com/zh-Hans-CN/index/sora-2/>, 2025.
- [31] William Peebles and Saining Xie. Scalable diffusion models with transformers. In [ICCV](#), pages 4195–4205, 2023.
- [32] Alec Radford, Jong Wook Kim, Tao Xu, Greg Brockman, Christine McLeavey, and Ilya Sutskever. Robust speech recognition via large-scale weak supervision. In [ICML](#), 2023.
- [33] Olaf Ronneberger, Philipp Fischer, and Thomas Brox. U-net: Convolutional networks for biomedical image segmentation. In [MICCAI](#), 2015.
- [34] Ludan Ruan, Yiyang Ma, Huan Yang, Huiguo He, Bei Liu, Jianlong Fu, Nicholas Jing Yuan, Qin Jin, and Baining Guo. Mm-diffusion: Learning multi-modal diffusion models for joint audio and video generation. In [CVPR](#), 2023.
- [35] Sizhe Shan, Qiulin Li, Yutao Cui, Miles Yang, Yuehai Wang, Qun Yang, Jin Zhou, and Zhao Zhong. Hunyuanvideo-foley: Multimodal diffusion with representation alignment for high-fidelity foley audio generation. [arXiv preprint arXiv:2508.16930](#), 2025.
- [36] Oriane Siméoni, Huy V Vo, Maximilian Seitzer, Federico Baldassarre, Maxime Oquab, Cijo Jose, Vasil Khalidov, Marc Szafraniec, Seungeun Yi, Michaël Ramamonjisoa, et al. Dinov3. [arXiv preprint arXiv:2508.10104](#), 2025.
- [37] Zachary Teed and Jia Deng. Raft: Recurrent all-pairs field transforms for optical flow. In [ECCV](#), 2020.
- [38] Andros Tjandra, Yi-Chiao Wu, Baishan Guo, John Hoffman, Brian Ellis, Apoorv Vyas, Bowen Shi, Sanyuan Chen, Matt Le, Nick Zacharov, et al. Meta audiobox aesthetics: Unified automatic quality assessment for speech, music, and sound. [arXiv preprint arXiv:2502.05139](#), 2025.
- [39] Ang Wang, Baole Ai, Bin Wen, Chaojie Mao, Chen-Wei Xie, Di Chen, Feiwu Yu, Haiming Zhao, Jianxiao Yang, Jianyuan Zeng, et al. Wan: Open and advanced large-scale video generative models. [arXiv preprint arXiv:2503.20314](#), 2025.
- [40] Duomin Wang, Wei Zuo, Aojie Li, Ling-Hao Chen, Xinyao Liao, Deyu Zhou, Zixin Yin, Xili Dai, Daxin Jiang, and Gang Yu. Universe-1: Unified audio-video generation via stitching of experts. [arXiv preprint arXiv:2509.06155](#), 2025.

- [41] Jun Wang, Xijuan Zeng, Chunyu Qiang, Ruilong Chen, Shiyao Wang, Le Wang, Wangjing Zhou, Pengfei Cai, Jiahui Zhao, Nan Li, et al. Kling-foley: Multimodal diffusion transformer for high-quality video-to-audio generation. [arXiv preprint arXiv:2506.19774](#), 2025.
- [42] Kai Wang, Shijian Deng, Jing Shi, Dimitrios Hatzinakos, and Yapeng Tian. Av-dit: Taming image diffusion transformers for efficient joint audio and video generation. In [ACM Multi](#), 2025.
- [43] Le Wang, Jun Wang, Chunyu Qiang, Feng Deng, Chen Zhang, Di Zhang, and Kun Gai. Audiogen-omni: A unified multimodal diffusion transformer for video-synchronized audio, speech, and song generation. [arXiv preprint arXiv:2508.00733](#), 2025.
- [44] Mengchao Wang, Qiang Wang, Fan Jiang, Yaqi Fan, Yunpeng Zhang, Yonggang Qi, Kun Zhao, and Mu Xu. Fantasytalking: Realistic talking portrait generation via coherent motion synthesis. In [ACM Multi](#), 2025.
- [45] Yi Wang, Yanan He, Yizhuo Li, Kunchang Li, Jiashuo Yu, Xin Ma, Xinhao Li, Guo Chen, Xinyuan Chen, Yaohui Wang, et al. Internvid: A large-scale video-text dataset for multimodal understanding and generation. [arXiv preprint arXiv:2307.06942](#), 2023.
- [46] Yusong Wu, Ke Chen, Tianyu Zhang, Yuchen Hui, Taylor Berg-Kirkpatrick, and Shlomo Dubnov. Large-scale contrastive language-audio pretraining with feature fusion and keyword-to-caption augmentation. In [ICASSP](#), 2023.
- [47] Yazhou Xing, Yingqing He, Zeyue Tian, Xintao Wang, and Qifeng Chen. Seeing and hearing: Open-domain visual-audio generation with diffusion latent aligners. In [CVPR](#), pages 7151–7161, 2024.
- [48] An Yang, Baosong Yang, Beichen Zhang, Binyuan Hui, Bo Zheng, Bowen Yu, Chengyuan Li, Dayiheng Liu, Fei Huang, Haoran Wei, Huan Lin, Jian Yang, Jianhong Tu, Jianwei Zhang, Jianxin Yang, Jiaxi Yang, Jingren Zhou, Junyang Lin, Kai Dang, Keming Lu, Keqin Bao, Kexin Yang, Le Yu, Mei Li, Mingfeng Xue, Pei Zhang, Qin Zhu, Rui Men, Runji Lin, Tianhao Li, Tingyu Xia, Xingzhang Ren, Xuancheng Ren, Yang Fan, Yang Su, Yichang Zhang, Yu Wan, Yuqiong Liu, Zeyu Cui, Zhenru Zhang, and Zihan Qiu. Qwen2.5 technical report. [arXiv preprint arXiv:2412.15115](#), 2024.
- [49] Sidi Yang, Tianhe Wu, Shuwei Shi, Shanshan Lao, Yuan Gong, Mingdeng Cao, Jiahao Wang, and Yujiu Yang. Maniq: Multi-dimension attention network for no-reference image quality assessment. In [CVPR](#), 2022.
- [50] Zhuoyi Yang, Jiayan Teng, Wendi Zheng, Ming Ding, Shiyu Huang, Jiazheng Xu, Yuanming Yang, Wenyi Hong, Xiaohan Zhang, Guanyu Feng, et al. Cogvideox: Text-to-video diffusion models with an expert transformer. [arXiv preprint arXiv:2408.06072](#), 2024.
- [51] Liping Yuan, Jiawei Wang, Haomiao Sun, Yuchen Zhang, and Yuan Lin. Tarsier2: Advancing large vision-language models from detailed video description to comprehensive video understanding. [arXiv preprint arXiv:2501.07888](#), 2025.
- [52] Guozhen Zhang, Zixiang Zhou, Teng Hu, Ziqiao Peng, Youliang Zhang, Yi Chen, Yuan Zhou, Qinglin Lu, and Limin Wang. Uniavgen: Unified audio and video generation with asymmetric cross-modal interactions. [arXiv preprint arXiv:2511.03334](#), 2025.
- [53] Yifu Zhang, Hao Yang, Yuqi Zhang, Yifei Hu, Fengda Zhu, Chuang Lin, Xiaofeng Mei, Yi Jiang, Bingyue Peng, and Zehuan Yuan. Waver: Wave your way to lifelike video generation. [arXiv preprint arXiv:2508.15761](#), 2025.
- [54] Yiming Zhang, Yicheng Gu, Yanhong Zeng, Zhening Xing, Yuancheng Wang, Zhizheng Wu, and Kai Chen. Foleyrafter: Bring silent videos to life with lifelike and synchronized sounds. [arXiv preprint arXiv:2407.01494](#), 2024.
- [55] Lei Zhao, Linfeng Feng, Dongxu Ge, Fangqiu Yi, Chi Zhang, Xiao-Lei Zhang, and Xuelong Li. Uniform: A unified diffusion transformer for audio-video generation. [arXiv e-prints](#), 2025.

Appendix

A Mouth-Area Mask Validation

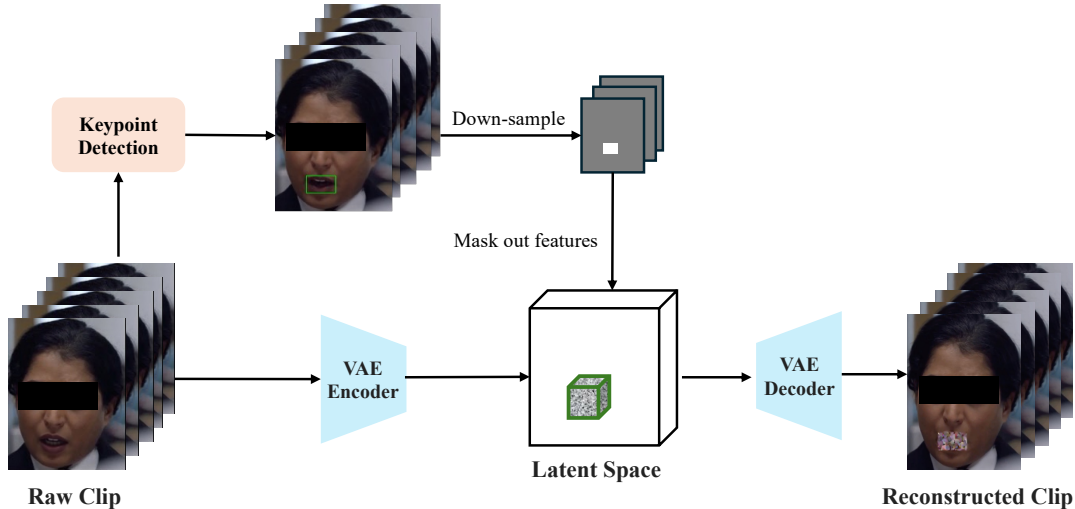


Figure 6 Mouth-area mask generation and validation pipeline. Detected mouth regions are mapped to VAE latent space, then zero-masked and decoded to verify localization accuracy through selective visual degradation. The eyes have been obscured to protect the subject’s identity.

To validate our mouth-area localization strategy, we perform zero-masking experiments in the VAE latent space. As illustrated in Fig. 6, we first detect facial keypoints to localize the mouth region with a bounding box, map this box to VAE latent space considering spatial downsampling and temporal merging, set the corresponding latent features to zero, and finally decode back to pixel space. Accurate localization should result in degradation exclusively in the mouth area while preserving other regions.

Fig. 7 presents validation results across four different video samples. For each sample, we compare the original frames with detected mouth boxes (top row) against the reconstructed frames from zero-masked latents (bottom row). As shown in the reconstructed sequences, the mouth regions exhibit clear visual degradation (blurring or distortion), while other facial features such as eyes, nose, and overall face structure remain well-preserved. This selective degradation pattern across different subjects, poses, and expressions confirms that our spatial-temporal downsampling approach accurately preserves mouth localization when mapping from pixel space to VAE latent space. The precise alignment validates that the mouth-aware loss applies targeted supervision to the correct region for effective lip-speech synchronization learning.



Figure 7 Zero-masking validation results across four video samples. For each sample, the top row shows the original video frames with detected mouth bounding boxes (green), and the bottom row shows the reconstructed frames after zero-masking the corresponding region in VAE latent space. The selective degradation observed exclusively in the mouth areas of reconstructed frames confirms precise mask localization. Best viewed with zoom in. The eyes have been obscured to protect the subject’s identity.